

The Beta Drift of Three-Dimensional Vortices: A Numerical Study

BIN WANG AND XIAOFAN LI

Department of Meteorology, School of Ocean and Earth Sciences and Technology, University of Hawaii at Manoa, Honolulu, Hawaii

(Manuscript received 20 March 1991, in final form 12 August 1991)

ABSTRACT

The beta effect on translation of cyclonic and anticyclonic vortices with height-dependent circulation (the beta-drift problem) is investigated via numerical experiments using a dry version of a multilevel primitive equation model (Florida State University model).

The vertical structure of vortex circulation influences steady translation in a manner similar to that of the horizontal structure. Both spatially change the mean relative angular momentum (MRAM) of the vortex. The translation speed and its meridional component are both approximately proportional to the square root of the magnitude of MRAM of the initial (or quasi-steady-state) symmetric circulation. The latitude is another important factor controlling the speed of the beta drift. The meridional component decreases by about 45% when the central latitude of the vortex increases from 10° to 30°N .

The beta-drift speed is intimately related to the axially asymmetric pressure field. During quasi-steady vortex translation the asymmetric pressure field maintains a stationary wavenumber 1 pattern in azimuthal direction with a high in the northeast and a low in the southwest quadrant of a Northern Hemisphere cyclone. The beta-drift velocity is approximately equal to the geostrophic flow implied by the asymmetric pressure gradient at the vortex center. If the Rossby number associated with the asymmetric flow is small, to the lowest order, the asymmetric pressure gradient force at the vortex center is balanced by the Coriolis force associated with the beta drift of the vortex.

1. Introduction

Beta drift is a basic component of tropical cyclone motion. It arises from the interaction between the gradient of earth's vorticity (or in more general terms, the absolute-vorticity gradient) and the vortex circulation. Beta drift may create a deviation from environmental steering and may play a dominant role if the ambient steering current is weak or indefinite, particularly in the deep tropics. Study of beta drift also provides fundamental understanding of nonlinear interaction between the vortex dynamics and the environment.

The investigation of motion of an isolated barotropic vortex in a quiescent environment dates back to Rossby (1948). Using a solid-body-rotation vortex and assuming a balance between the integrated pressure force by the surrounding fluid and the Coriolis force associated with the vortex translation, Rossby argued that an axially symmetric cyclonic vortex is driven poleward due to the latitudinal variation of the Coriolis parameter. Adem (1956) reexamined the translation of a geostrophic vortex on beta plane in terms of a Taylor expansion of streamfunction in time. In the Northern

Hemisphere, a cyclonic vortex was shown to first move westward then turn northward. Adem first noticed a relation between vortex translation and its horizontal structure: the initial westward and subsequent northward components are proportional to the vortex radius and the maximum wind speed, respectively.

Numerical experiments using barotropic models all indicate that an initially symmetric vortex on a beta plane moves consistently northwestward in the Northern Hemisphere (e.g., Anthes and Hoke 1975; Madala and Piacsek 1975) rather than northward or first westward then northward. Recent numerical studies of barotropic beta drift have further focused on the effects of the horizontal vortex structure on the beta drift. DeMaria (1985) showed that the vortex track is much more sensitive to changes in the outer region (size change) than to changes in the inner regions (intensity change). Holland (1983, 1984) postulated that the vortex motion depends on cyclone-environment interaction at an effective radius of interaction, which is an envelope defined by the region of rapid increase in inertial instability. He intuitively predicted that the maximum wind variation should not affect the motion, while the changes in the size and strength of the outer circulation affect the motion by changing the effective radius. On the other hand, Chan and Williams (1987) showed that for a constant-shape vortex the northward movement increases with both the maximum wind

Corresponding author address: Dr. Bin Wang, University of Hawaii, School of Ocean & Earth Science & Technology, 2525 Correa Rd, Honolulu, HI 96822.

speed and the radius of maximum wind. Fiorino and Elsberry (1989a) examined contributions of small-, medium-, and large-scale components of some typical tangential wind profiles to the vortex motion. They concluded that the speed of the motion is primarily determined by the strength of large-scale components (the flow in the outer region), whereas the medium (and small) scales have a significant effect on the direction of the motion by influencing the orientation of the asymmetric gyres that are induced mainly by the large scales.

Rossby's theoretical explanation of beta drift was based on the analysis of resultant force and energetics of a solid-body-rotation vortex in which asymmetric vortex circulation was not permitted. However, vortex translation is closely related to this asymmetric circulation. The asymmetric gyres associated with translation were termed *beta gyres* since they arise from the beta effect (or the effect of the absolute-vorticity gradient) (Fiorino and Elsberry 1989b). Fiorino and Elsberry found a close association of the speed and direction of the vortex motion with the asymmetric flow at the vortex center (the ventilation flow).

In his linear analysis, Willoughby (1988) derived a proportionality of the northward speed to the initial total relative angular momentum (TRAM) in the presence of asymmetric circulation. However, Shapiro and Ooyama (1990) pointed out that for an initial symmetric vortex with nonzero TRAM, the TRAM within a large circle centered on the vortex would decrease with time due to Rossby wave dispersion (McWilliams and Flierl 1979), and thus the motion of the vortex could not be related to the initial TRAM in any simple way.

Identification of controlling factors responsible for beta drift remains a necessary step toward understanding the beta-drift dynamics. In this regard, previous analyses using different barotropic models and approaches have not reached a generally accepted conclusion. In addition, the study of the beta drift has been primarily confined to the framework of barotropic models. However, the structure of tropical cyclones is height dependent. It is not clear how the vertical structure of the circulation influences vortex motion.

The present study uses numerical experiments to study beta drift of vortices with height-dependent structure. Section 2 briefly introduces the numerical model and results of sensitivity tests. Our first focus is to identify possible dynamic factors and processes that are responsible for the beta drift, in particular, the influence of the vertical structure of vortex on its motion (section 3). The second focus is to examine the relation between the axially asymmetric pressure field and the beta drift, as well as the initial symmetric vortex circulation, in an effort to explain the mechanism for beta drift (section 4). The last section summarizes our primary findings.

2. The model and sensitivity tests

a. The numerical model

The model is based on Florida State University (FSU) regional model, which is a multilayer, primitive equation model in sigma coordinates. Semi-Lagrangian and semi-implicit schemes were applied to an Arakawa C-type staggered grid (Krishnamurti et al., 1990). To consider a simple system that contains only the fundamental elements of the beta drift, diabatic heating and other moist processes have intentionally been excluded.

Sponge layers are applied to the model's lateral boundaries. Any dependent variable at l th layer from the boundary is

$$X_n(I) = W(I)X_n(I) + [1.0 - W(I)]X_p(I),$$

$$I = 0, 1, 2, \dots, \quad (1)$$

where the subscripts n and p denote current value and the value at a previous time step, respectively; $W(I)$ is a weighting coefficient, which takes increasing values 0.0, 0.546, 0.794, 0.907, 0.958, and 0.981 for boundary grid points $I = 0, 1, 2, 3, 4, 5$, and 1.0 for all interior grid points.

The initial fields consist of a finite-size symmetric vortex embedded in a quiescent environment. The tangential wind profile for cyclones is given by

$$V_\lambda(r) = - \begin{cases} V_m \frac{r}{r_m} \left\{ \exp \left\{ \frac{1}{b} \left[1 - \left(\frac{r}{r_m} \right)^b \right] \right\} \right\} \\ - \frac{|r - r_m|}{R_0 - r_m} \exp \left\{ \frac{1}{b} \left[1 - \left(\frac{R_0}{r_m} \right)^b \right] \right\} \right\}, \\ r \leq R_0, \quad 0, \quad r > R_0, \end{cases} \quad (2)$$

where r denotes radial distance from the vortex center. There are four characteristic parameters in (2): V_m and r_m represent the maximum wind speed and the radius of maximum wind (RMW), respectively, R_0 is the radius of the vortex, and b is a parameter determining the shape of the wind profile. Figure 1a shows several examples of tangential wind profiles for cyclones described by (2). The vertical wind profile is similar to the observed profile (Frank 1977):

$$v_p(p) = \begin{cases} \frac{(v_2 - v_1)p - p_1v_2 + p_2v_1}{p_2 - p_1} & p_1 \leq p < p_2 \\ \frac{(v_3 - v_2)p - p_2v_3 + p_3v_2}{p_2 - p_3} & p_2 \leq p < p_3 \\ \frac{(v_3 - v_4)p - p_4v_3 + p_3v_4}{p_3 - p_4} & p_3 \leq p \leq p_4, \end{cases} \quad (3)$$

where p is nondimensional pressure normalized by 1000 mb; and v_1, v_2, v_3 , and v_4 are nondimensional

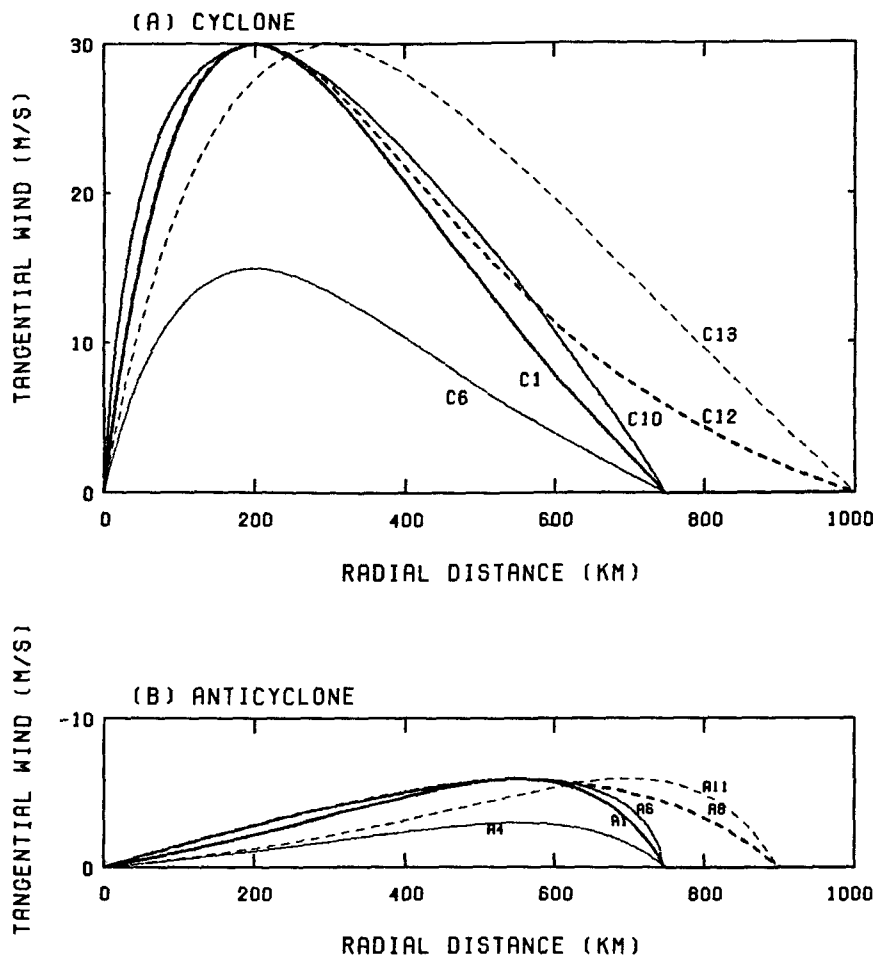


FIG. 1. Azimuthal wind profiles for (a) cyclones described by (2) and (b) anticyclones described by (5). Parameter values for experiments C1, C6, C10, C12, and C13 are given in Table 3a and for experiments A1, A4, A6, A8, and A11 are given in Table 3b. The thick solid curves denote the standard profiles.

tangential wind speeds normalized by the maximum tangential wind speed v_m at nondimensional pressure levels $p_1 = 0.1$, $p_2 = 0.25$, $p_3 = 0.85$, and $p_4 = 1.0$, respectively. Several examples of vertical wind profiles described by (3) are given in Fig. 2a.

In the following discussion, a standard wind profile is a profile with the following parameters in (2) and (3): $v_m = 30 \text{ m s}^{-1}$, $R_o = 750 \text{ km}$, $r_m = 200 \text{ km}$, $b = 1.0$, $v_1 = 0.0$, $v_2 = 0.68$, $v_3 = 1.0$, and $v_4 = 0.83$. This standard profile is depicted by thick solid curves in Figs. 1a and 2a.

The initial geopotential height field inside the vortex is calculated using the gradient-wind relationship, while outside the vortex we assume a typical structure for a tropical environment in hurricane season (Jordan 1958).

Precise and objective determination of the central track is important for the calculation of the beta-drift

velocity. The center of the cyclonic vortex is defined by minimum surface pressure that is determined by a method similar to that used by Wang and Zhu (1989). In this method, fine gridpoint values and quadratic functions of the zonal and meridional ordinates are used to compute the location of the cyclone center objectively and accurately. For anticyclones, due to the flatness of the pressure field, near the center the determination of the central location from the pressure field is much less reliable. We therefore use the wind field to first construct the maximum wind belt then determine the central location geometrically.

Identification of the asymmetric circulation requires partition of the total circulation into a symmetric and an asymmetric component. The decomposition procedure is similar to that used by Fiorino and Elsberry (1989a). The difference is in the method determining the vortex center. In the present model, the minimum

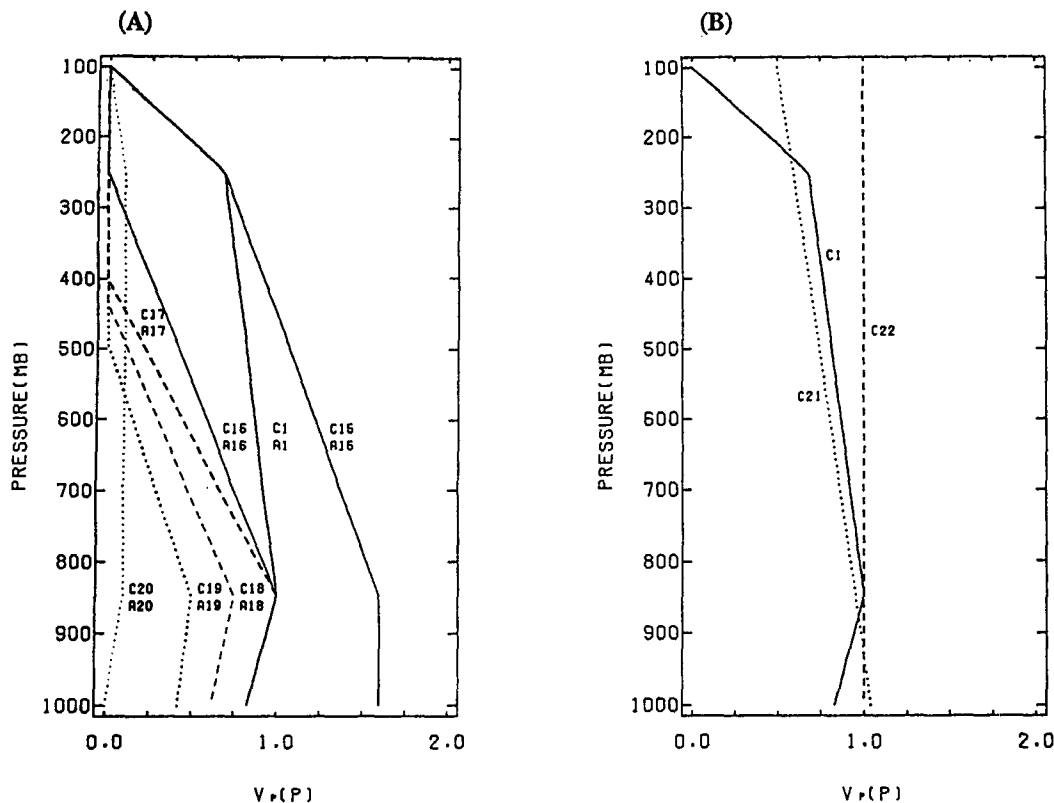


FIG. 2. (a) Vertical profiles of azimuthal wind described by (3). These profiles are used for cases C1 (A1), C15 (A15), C16 (A16), C17 (A17), C18 (A18), C19 (A19), and C20 (A20), respectively. The thick solid curves denote the standard vertical profiles; (b) as (a) except for cases C21 and C22.

pressure at the surface is defined as the vortex center. Cubic splines were employed to interpolate the model solution into a fine mesh of 20 km. The fine mesh was then transformed into cylindrical coordinates.

b. Sensitivity experiments

Sensitivities of the numerical solution to viscosity, lateral boundary conditions, domain size, and horizontal resolution were tested. Since six- and three-level models yielded similar results, a three-level model was used for the sensitivity tests. The standard vertical and horizontal wind profiles were adopted for the initial vortices. All integration were continued up to 48 h.

Experiments with three different horizontal viscosity coefficients ($A_H = 0, 1000, 8000 \text{ m}^2 \text{ s}^{-1}$) indicate that the differences in direction are within 8° and in speed are less than 0.12 m s^{-1} . The vortex motion is thus not sensitive to the values of viscosity coefficient in the range of $0\text{--}10^4 \text{ m}^2 \text{ s}^{-1}$. This is probably due to the presence of sufficient inherent dissipation within the semi-Lagrangian advection scheme (e.g., McCalpin 1988). Two different lateral boundary conditions were tested: one with sponge layers and the other with fixed

boundary condition. No appreciable difference was found between the two tests as long as the domain size was sufficiently large.

Three square domains with sidelengths of 2000, 3120, and 3920 km are used to test the sensitivity of the solution to domain size. In these experiments, the radius of the initial vortex is 750 km and the beta-drift speed is about $100\text{--}200 \text{ km day}^{-1}$. The tracks of vortex centers in two larger-domain (3120 and 3920 km) experiments are very similar, but appreciably different from that of the smallest domain (2000 km) experiment. It appears that in order to avoid the influences of the lateral boundaries, an adequate domain size for 48-h integration is at least twice the vortex size. This has an important implication for the effects of Rossby wave dispersion. Even though the initial cyclonic circulation has a finite size with radius of R_0 , the radiation of Rossby waves continuously diminishes the cyclonic circulation and creates a weak anticyclonic circulation outside the cyclonic circulation. The anticyclonic circulation, albeit weak, has large negative angular momentum. This causes a dramatic change in the total relative angular momentum of the vortex when all the weak anticyclonic circulation is taken into account

(Shapiro and Ooyama 1990). This result emphasizes that the weak surrounding anticyclonic circulation outside the circle with a radius of $2R_0$ centered at the vortex center has negligible effect on the vortex motion for a 48-h simulation.

The model horizontal resolution is another crucial parameter. Two groups of tests were conducted. The RMWs of the vortex were 100 and 200 km, respectively. With increasing resolution, both the speed and direction tend to approach a constant limit for fixed RMW (Table 1), implying that the numerical simulation yields a convergent solution as resolution increases. In addition, simulations with higher resolution show less oscillatory behavior in vortex tracks because in those simulations the maximum wind and inner wind profile can be better resolved and the vortex center can be better caught. An adequate horizontal resolution for simulation depends on the RMW because a large ratio of horizontal resolution to RMW would result in rapid dispersion of the vorticity maximum in finite-difference models (DeMaria 1985). In order to obtain a reasonably approximate solution, our results suggest that the horizontal resolution should be less than about 40% of the RMW of initial vortex. Large errors could arise if the horizontal resolution cannot resolve RMW properly.

3. Dynamic factors controlling the beta drift

In numerical integration of the present model, the vortex initially accelerates then assumes a near-steady translation. This can be seen from Table 2a, which presents the mean speed and its zonal and meridional components averaged over each 12-h interval from initial time to hour 48. Given in Table 2b is the evolution of corresponding mean relative angular momentum (MRAM) of the cyclonic circulation of the vortex in the benchmark experiment. The MRAM is defined by

TABLE 2a. The evolution of the zonal, meridional, and total beta-drift speeds (m s^{-1}) in each 12-h interval averaged for 20 cyclonic vortices.

Hour	0–12	12–24	24–36	36–48
C_x (m s^{-1})	−0.37	−0.62	−0.74	−1.06
C_y (m s^{-1})	0.70	1.23	1.36	1.82
C (m s^{-1})	0.79	1.38	1.55	2.11

$$\text{MRAM} = \frac{\int_{p_t}^{p_0} \int_A V_\lambda(r) r dA dp}{\int_{p_t}^{p_0} \int_A dA dp}, \quad (4)$$

where $v_\lambda(r)$ is tangential speed of the initial vortex, A the horizontal area occupied by the initial vortex flow at level p , p_t and p_0 are the upper and lower boundaries of the vortex circulation, respectively. The initial acceleration occurs primarily during the first 12 h accompanied by a significant drop in the MRAM. For the variety of experiments carried out in this study, the ratio of the near-steady to initial MRAM is approximately a constant (80%). This adjustment period is much shorter than the normal day or two in barotropic models. From hour 12 to 36, the beta drift tends to be near steady with a slow increase in drifting speed and an insignificant decrease in MRAM. After 36 h the drift speed starts to increase significantly due to the growth of the asymmetric circulation component. In what follows, the mean drift speed is defined as the speed averaged over the quasi-steady translation phase from hour 12 to hour 36.

The meridional component of the beta-drift velocity depends upon the signs of both the relative vorticity and the Coriolis parameter. It is directed northward for cyclones and southward for anticyclones in the Northern Hemisphere and the opposite is true in the Southern Hemisphere. The zonal component of beta drift, however, is always directed westward regardless of the signs of vorticity and the Coriolis parameter.

a. The dependence of the meridional beta drift on the horizontal structure of the initial vortex

First, the dependence of meridional component of the beta drift on horizontal circulation of a finite-size cyclonic vortex was examined. For this purpose, vertical structure was fixed (the same as standard wind

TABLE 1. Dependence of the mean translation speed and direction on the model horizontal resolution Δx for RMW = 100 and 200 km, respectively. The direction is measured from the north counterclockwise. The mean translation velocity is averaged over the period from hour 12 to 36 for cyclonic cases.

Δx (km)	Speed (m s^{-1})	Direction ($^\circ$)
RMW = 100 km		
80	1.41	42.0
60	2.05	26.7
40	1.96	34.8
RMW = 200 km		
160	1.40	14.9
120	1.93	26.5
80	2.05	25.6

TABLE 2b. The evolution of the ratio of the instant to initial mean relative angular momentum in the benchmark equipment.

Hour	6	18	30	42
MRAM	0.831	0.808	0.793	0.76

profile), while different azimuthal wind profiles for the initial vortex were tested. Table 3a lists values for four key parameters for each of these experiments along with the mean drift speeds. Case C1 is the benchmark experiment that uses the standard profile. In cases C2–C9, only maximum wind speed varies. Similarly, in cases C10 and C11 only parameter b changes; in case C12 only the radius of vortex. Cases C13 and C14 have more than one parameter different from the standard profile.

The poleward-drift speed increases with increasing maximum wind speed (cf. experiments C1–C9). This is in general agreement with the result derived from a barotropic model for an infinite-size cyclonic vortex (Chan and Williams 1987). Second, the stronger the azimuthal wind in the outer flow region (corresponding to a smaller b , see Fig. 1a), the faster the poleward drift (cf. experiments C1, C10, and C11). Finally, the poleward-drift speed increases with expanding vortex size (compare experiment C1 with C12) and with increasing RMW (cf. experiment C12 and C13).

Increases in the maximum wind speed, RMW, and vortex size and/or the decrease in parameter b all imply an increase in MRAM. Therefore, the foregoing results suggest that the northward translation generally becomes faster when MRAM increases (Table 3a). Notice that the MRAM is an integrated quantity whose integrand is a quadratic function in radial distance from vortex center. It follows that changes in the outer part of tangential wind distribution could dramatically alter MRAM. This is consistent with the previous finding that changes in the outer flow of the initial vortex significantly influence vortex motion (DeMaria 1985; Fiorino and Elsberry 1989b).

As MRAM approaches zero the northward speed tends to vanish. It is, therefore, interesting to consider

the case in which MRAM reverses its sign (an anticyclonic vortex). Due to the restriction by gradient-wind balance, the horizontal structure for anticyclonic vortices must differ from that for cyclonic vortices. The tangential wind profile for an anticyclone is given by

$$v_{\lambda}(r) = \begin{cases} V_m \frac{R_0 - r}{R_0 - r_m} \left\{ \exp \left\{ \frac{1}{b} \left[1 - \left(\frac{R_0 - r}{R_0 - r_m} \right)^b \right] \right\} \right\} \\ - \frac{|r - r_m|}{r_m} \exp \left\{ \frac{1}{b} \left[1 - \left(\frac{R_0}{R_0 - r_m} \right)^b \right] \right\} \right\}, & r \leq R_0, \\ 0, & r > R_0, \end{cases} \quad (5)$$

where parameters v_m , R_0 , r_m , b , and r have the same meaning as in (2), but the maximum wind speed is restricted. Figure 1b illustrates several examples of azimuthal wind profiles for anticyclones.

Fourteen anticyclones with different horizontal structures and identical vertical wind profile were studied. These cases are listed in Table 3b in terms of characteristic parameters in azimuthal wind profiles. The southward-drift speed is indeed well correlated with the anticyclonic MRAM, although the correlation is not as good as that for cyclones. This is clearly seen from the closed dots in Fig. 3a.

b. The dependence of the meridional beta drift on the vertical structure of the vortex

One way to verify the relationship between initial MRAM and the quasi-steady meridional beta-drift speed in a multilevel model is to examine the impacts of change of vertical profile of azimuthal wind on its motion, because change of the vertical profile of azimuthal wind would effectively change the MRAM even though the horizontal structure remains the same. A simple test was carried out in which two cyclones were considered. Each had an identical horizontal wind profile to that in the benchmark experiment but different vertical profiles as shown by cases C21 and C22 in Fig. 2b. In case C21 and the benchmark experiment C1, the initial cyclones have identical MRAM. The beta-drift speeds are almost identical (In Fig. 3, C21 overlaps the benchmark experiment), suggesting that the beta-drift speed depends only upon the vertical mean RAM. In case C22, the MRAM of the initial vortex is larger than that in that benchmark experiment. Correspondingly, the beta-drift speed in case C22 is faster than that of the benchmark experiment (Fig. 3c).

To further verify this finding, a six-level model was used and six different vertical wind profiles for cyclones (C15–C20) and anticyclones (A15–A20), which are shown in Fig. 2a, were constructed. In these experiments, the azimuthal wind profile of the initial vortex

TABLE 3a. Parameters for azimuthal wind profile of initial vortices, mean relative angular momentum (MRAM), and the zonal and meridional beta-drift speed for cyclonic vortices with different horizontal structure. The asterisk denotes a parameter that is the same as that of the standard case C1.

Case	V_m (m s^{-1})	r_m (km)	b	R_0 (km)	MRAM ($10^6 \text{ m}^2 \text{ s}^{-1}$)	C_x (m s^{-1})	C_y (m s^{-1})
C1	30	200	1.0	750	4.02	−0.83	1.85
C2	50	*	*	*	6.69	−1.28	2.39
C3	45	*	*	*	6.02	−1.22	2.38
C4	39	*	*	*	5.22	−1.23	2.28
C5	20	*	*	*	2.68	−0.84	1.45
C6	15	*	*	*	2.01	−0.89	1.25
C7	10	*	*	*	1.34	−0.76	1.19
C8	5	*	*	*	0.67	−0.43	0.82
C9	2	*	*	*	0.27	−0.25	0.29
C10	*	*	0.5	*	4.76	−0.74	2.04
C11	*	*	2.0	*	2.12	−0.84	1.51
C12	*	*	*	1000	3.63	−1.11	2.02
C13	*	300	*	1000	6.01	−1.47	2.26
C14	20	*	0.5	*	3.17	−0.75	1.47

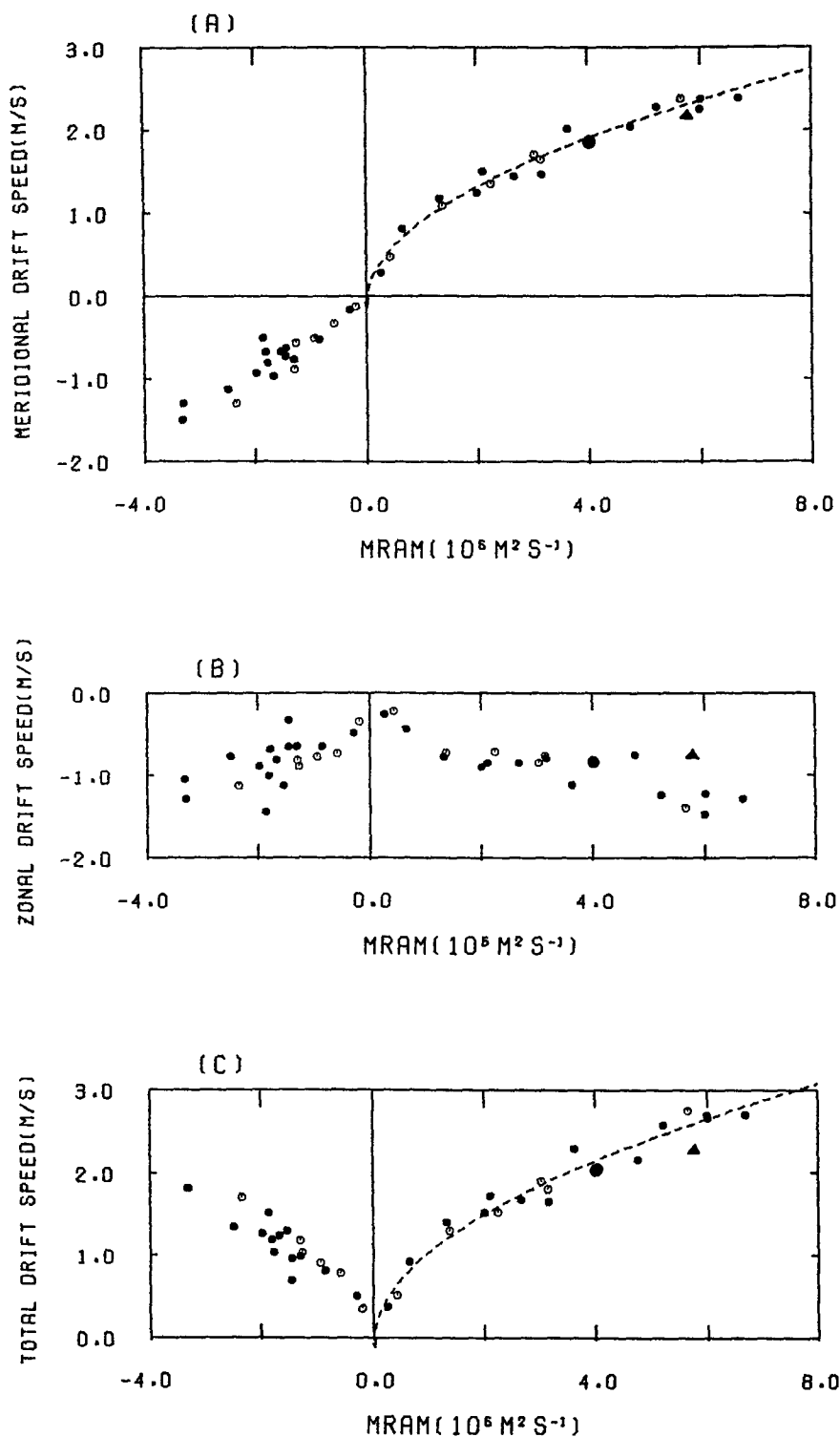


FIG. 3. (a) Mean meridional drift speed, (b) mean zonal drift speed, and (c) mean total drift speed at hour 24 as a function of initial mean relative angular momentum (MRAM) for 42 experiments. Dashed line in (a) is the regression curve given by (6). The closed (open) dots represent those experiments in which the vertical (horizontal) wind profile is fixed. The big closed dot denotes the benchmark experiment and the triangle denotes case C22.

have the same parameters as the standard ones except for the maximum wind speed. The relationship between the MRAM of the initial vortex and the meridional drift speed for these cases are shown in Fig. 3a by open dots. Apparently, the vertical structure affects the beta drift by changing the MRAM in a similar manner as does the horizontal structure. This confirms that the MRAM of the initial vortex is a controlling factor for the meridional beta drift.

The relationship between the MRAM (in units of $10^6 \text{ m}^2 \text{ s}^{-1}$) and the meridional beta-drift speed (m s^{-1}) is essentially nonlinear. Using the results from all 42 experiments the northward drift speed may be approximated by

$$C_y = a|\text{MRAM}|^{1/2} + b, \quad (6)$$

where the coefficients a and b are, respectively, 1.01, -0.11 for cyclones and -0.92 , 0.36 for anticyclones. This nonlinear relationship fits better for a cyclonic vortex than for an anticyclonic vortex: regression equation (6) reduces the total sample variance by 96.9% for cyclones and 83.8% for anticyclones. Both exceed the 99% confidence level.

The dependence of the beta drift on the vertical mean relative angular momentum is caused by the vertical coupling of the vortex circulation through vertical mo-

tion. To further examine this vertical coupling, four additional experiments were performed using a ten-level model. In the first two experiments, the vortices have cyclonic circulation through the entire vertical domain from 1000 to 100 mb. In spite of the large difference in RAM at different levels, the meridional beta-drift speeds at each level are nearly the same (Figs. 4a and 4b). This indicates that for a deep cyclone with height-dependent azimuthal wind profile, the secondary circulation can maintain its integral structure, and the vortex translates at a speed proportional to vertical mean RAM. In the third experiment, the initial cyclone has the same circulation structure as the first experiment (Fig. 4a) but the static stability was reduced by about an order of magnitude. The corresponding vertical motion at the midlevel in the third experiment increases by a factor of 8. The resultant beta-drift speed is almost identical to that of the first experiment. This suggests that the vertical motion in the standard stability case is strong enough to couple the deep vortex circulation vertically.

The fourth experiment deals with a "compound" baroclinic vortex that has cyclonic circulation in low levels (1000–550 mb) and anticyclonic circulation aloft (550–100 mb). For such a compound vortex with vorticity changing sign at a middle level, when the Coriolis

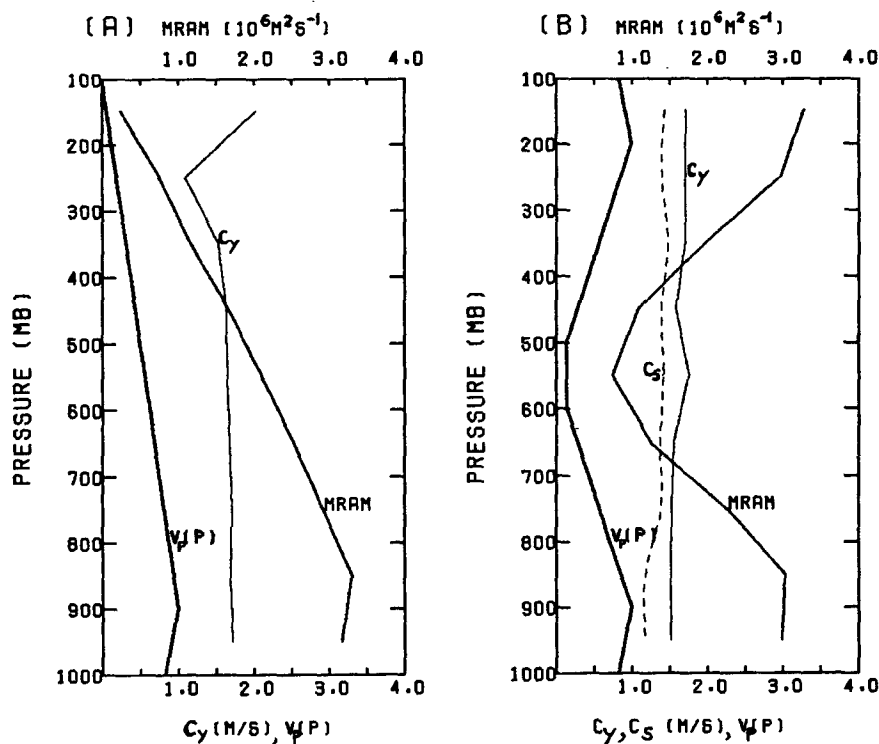


FIG. 4. Vertical variations of the MRAM and the mean meridional drift speed C_y at hour 24 for two vortices with different initial vertical wind profile $v_p(p)$. The dashed line (C_s) represents the mean geostrophic wind speed implied by the asymmetric pressure gradient at the vortex center.

parameter is positive, the anticyclonic part moves west-southwestward while the cyclonic part moves north-northwestward. The movement of the upper and lower parts are almost completely independent of each other. This has been demonstrated by a controlled experiment in which a cyclonic vortex has an identical structure with the lower part of the compound vortex but without an upper-level anticyclone. The motion of this "pure" cyclonic vortex is nearly the same as that of the cyclonic part of the compound vortex.

The separation of the upper anticyclonic and lower cyclonic parts of the compound vortex is due to the absence of vertical coupling between the two circulations. In the absence of diabatic heating as in the present case, the vertical motion associated with the divergent motion changes sign at the interface between the anticyclonic and cyclonic circulations. Thus, no vertical coupling holds the upper anticyclonic and lower cyclonic circulations together. Given convective heating, the vertical coupling might maintain an integral circulation system with positive vorticity below and negative vorticity aloft. In that case, the beta-drift tendency due to upper anticyclonic circulation would cancel the beta-drift tendency due to the low-level cyclonic circulation. The beta drift of the actual storm could substantially differ from a deep barotropic vortex.

c. The westward- and total beta-drift speeds

The westward-drift speed exhibits a weak linear correlation with absolute value of MRAM (Fig. 3b) for the selected samples. The correlation for cyclones is much better than that for anticyclones. Further careful examination of the dependence of westward-drift speed on vortex circulation leads to the following additional remarks.

1) The westward drift is faster for larger vortices. This is true for both cyclonic and anticyclonic vortices (comparing experiments C1 with C12 in Table 3a and experiments A1 with A8 in Table 3b).

2) For weak vortices ($V_m < 15 \text{ m s}^{-1}$), the westward-drift speed increases with increasing maximum wind speed. This can be seen from comparison of C6–C9 (Table 3a) and A1–A5 (Table 3b). However, for strong cyclonic vortices ($V_m \geq 15 \text{ m s}^{-1}$) the speed of westward drift has little to do with the maximum wind speed (C2–C4 in Table 3a).

Since the meridional beta-drift speed is, in general, larger than the zonal counterpart for cyclones and comparable for anticyclones, the total beta-drift speed for both cyclonic and anticyclonic vortices also displays a nonlinear relationship with the MRAM (Fig. 3c) similar to that between the meridional beta-drift speed and MRAM. For cyclones, this may be approximated by

$$C = 1.12|\text{MRAM}|^{1/2} - 0.091. \quad (7)$$

The total beta-drift speed is proportional to the square root of absolute value of MRAM with a linear correlation coefficient of 0.98.

d. Latitudinal dependence of beta drift

Kitade (1981) showed that the northward drift component varies with a nondimensional beta parameter, which was determined by the beta effect, vortex size, RMW, and intensity. For fixed vortex structures, say RMW = 200 km, vortex radius = 670 km, and $U_{\text{max}} = 30 \text{ m s}^{-1}$, when latitude increases from 10° to 30° , the nondimensional beta parameter decreases from 0.0065 to 0.0050 and the northward component of drift speed decreases by an insignificant amount (a few centimeters per second). Our results, however, indicate a much stronger latitudinal dependence of beta drift.

Three experiments were performed using a vortex with standard horizontal and vertical wind profile located initially at different latitudes: 10° , 20° , and 30°N . The meridional beta-drift speed is found to decrease by about 45% when initial latitude changes from 10°

TABLE 3b. As in Table 3a except for anticyclonic vortices.

Case	V_m (m s^{-1})	r_m (km)	b	R_0 (km)	MRAM ($10^6 \text{ m}^2 \text{ s}^{-1}$)	C_x (m s^{-1})	C_y (m s^{-1})
A1	−6	550	1.0	750	−1.66	−0.80	−0.96
A2	−12	*	*	*	−3.31	−1.04	−1.49
A3	−9	*	*	*	−2.49	−0.76	−1.12
A4	−3	*	*	*	−0.83	−0.64	−0.52
A5	−1	*	*	*	−0.28	−0.48	−0.16
A6	−6	*	0.5	*	−1.80	−1.00	−0.67
A7	−6	*	2.0	*	−1.44	−0.64	−0.72
A8	−6	*	*	900	−1.86	−1.44	−0.50
A9	−6	650	*	*	−1.44	−0.32	−0.62
A10	−6	450	*	*	−1.53	−1.12	−0.66
A11	−6	700	*	900	−1.98	−0.88	−0.92
A12	−6	400	*	600	−1.29	−0.64	−0.76
A13	−10	700	*	900	−3.30	−1.28	−1.29
A14	−6	600	*	800	−1.77	−0.67	−0.80

to 30°N (Table 4). Note that the decrease in beta parameter from 10° to 30°N is small (only about 11%), while the Coriolis parameter increases by a factor of 3. The latitudinal dependence of meridional beta drift could be a result of changes of both the beta and Coriolis parameters. On the other hand, the westward-drift speed does not seem to be related to changes in either beta or the Coriolis parameter in a simple monotonic way. As a result, when the initial vortex lies at lower latitudes, the vortex tends to move faster and more closely to a poleward direction.

The significant latitudinal dependence of the beta drift implies that a cyclonic vortex in the deep tropics has a relatively strong poleward motion tendency due to beta drift. Near the equator, where environmental steering flow is normally weak, beta-drift tendency may be a major mechanism for keeping a storm away from the equator.

4. The relationship between asymmetric pressure and beta drift

a. The beta effect-induced asymmetric circulation

Using a nondivergent barotropic model, Fiorino and Elsberry (1989a) demonstrated that the beta effect induces an initial asymmetric circulation (beta gyre). After a steady state is attained, the beta forcing is approximately balanced by the advection of asymmetric vorticity by the symmetric flow. The vorticity tendency that determines vortex motion is thus dominated by the advection of symmetric vorticity by the asymmetric flow. In particular, the area-mean asymmetric flow in the vicinity of the vortex center, which was termed as mean ventilation flow, appears to agree well with the beta-drift velocity.

The beta-induced asymmetric streamfunction observed in a reference frame fixed to the earth is dominated by a wavenumber 1 azimuthal component whose maximum and minimum are located near the outer boundary of the cyclonic circulation (Fig. 5). In the benchmark experiment as well as in other experiments, the intensity of the asymmetric gyre increases with time and the extent of the asymmetric circulation also slowly expands. More noticeably, the azimuthal phases of the asymmetric streamfunction centers vary slowly with time, implying a structural evolution of the beta gyre (Fig. 5). This can be seen also from the

TABLE 4. Dependence of the meridional (C_y), zonal (C_x), and total (C) beta-drift speed on the latitude of the initial vortex center. Terms β and f represent the β and f parameters at corresponding latitude.

Latitude (°N)	β ($10^{-11} \text{ m}^{-1} \text{ s}^{-1}$)	f (10^{-4} s^{-1})	C_y (m s^{-1})	C_x (m s^{-1})	C (m s^{-1})
10	2.25	0.25	2.74	-0.59	2.80
20	2.15	0.50	1.85	-0.83	2.03
30	1.98	0.73	1.51	-0.66	1.65

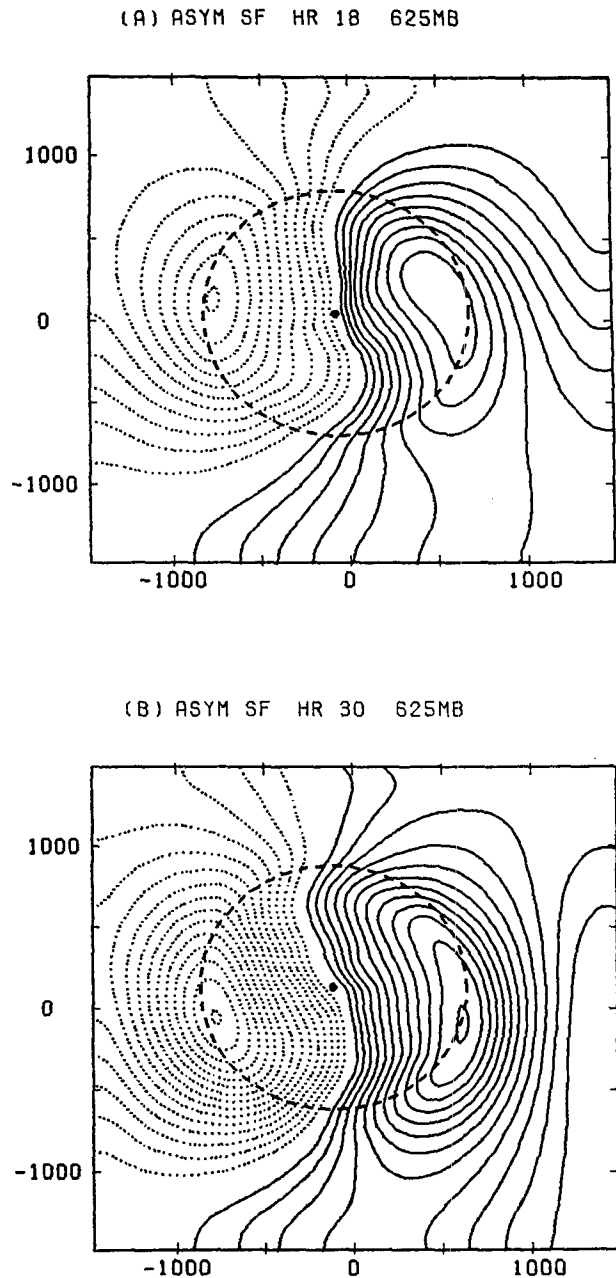


FIG. 5. The asymmetric stream function at 625 mb observed in a reference frame fixed to the earth in the benchmark experiment at (a) hour 18 and (b) hour 30. Solid (dashed) contours correspond to positive (negative) values from 0.5×10^5 (-0.5×10^5). The contour interval is $10^5 \text{ m}^2 \text{ s}^{-1}$. The closed dot denotes the vortex center, and the thick dashed circle denotes the boundary of the cyclonic circulation of the vortex. Units for abscissa and ordinate are kilometers.

change of the shape of the zero streamfunction line. In association with this structural evolution, the asymmetric flows near the vortex center change accordingly. The mean ventilation flow, therefore, crucially depends on the size of the circular area over which the asymmetric flow is averaged.

To facilitate discussion, the radius of the circular area over which the ventilation flow is defined is referred to as the radius of ventilation circle; an error vector is defined as the vectorial difference between the beta-drift velocity and the mean ventilation flow. The magnitude of the error vector at each level tends to reach a minimum when the radius of ventilation circle is between 240 and 400 km (Fig. 6). This implies an optimum radius for area-mean ventilation flow of about 320 km for the benchmark experiment. However, the optimum radius of ventilation circle depends on horizontal vortex structure. In particular, it tends to increase significantly with increasing MRAM (Fig. 7). This makes it difficult to define a mean ventilation flow and unambiguously determine the relationship between beta-drift speed and asymmetric circulation.

The asymmetric flow viewed from a reference frame moving with the vortex center is illustrated in Fig. 8. The asymmetric flow at the vortex center is vanishingly small and is relatively small over much of the cyclonic vortex (also see Smith et al. 1990; Shapiro and Ooyama 1990). The maximum asymmetric flows are located in a circular belt about 1000 km away from the center. Near the boundary of the cyclonic circulation there is a large radial gradient of asymmetric flow. Far away from the center (radial distance in excess of 1500 km) the asymmetric flow is essentially a constant velocity opposed to the beta-drift velocity. This asymmetric flow pattern viewed following a moving cyclone, to some extent, amounts to a flow field viewed from a solid cylinder that moves through a resting fluid with an equivalent beta-drift velocity. In Rossby's theoretical model such a solid-body-rotation vortex was adopted. Apparently Rossby's idealized model captures the first-order approximation of the real field. However, it precludes any penetrating asymmetric flow. The latter

is the fundamental difference between a solid-body-rotation vortex and a realistic cyclone.

b. The beta-induced asymmetric pressure field and the vortex motion

The pressure field is initially symmetric and in gradient wind balance with the symmetric vortex circulation. The interaction between vortex circulation and beta effect creates an asymmetric pressure field. This was first noticed by Anthes and Hoke (1975).

In contrast to the structural evolution of the asymmetric streamfunction, our experiments show that the asymmetric pressure (or geopotential height of the corresponding isobaric surface) field exhibits a quasi-steady structure: the azimuthal phases of the asymmetric pressure centers are almost time independent so that the asymmetric pressure pattern is stationary in the azimuthal direction (Fig. 9). The axis linking the maximum and minimum asymmetric pressure centers is persistently oriented in a northeast-southwest direction for the Northern Hemisphere with a high in the northeast quadrant and a low in the southwest quadrant. Therefore, the beta-drift velocity nearly aligns with the geostrophic wind implied by the asymmetric pressure field at the cyclone center.

To further quantify the relationship between vortex translation and asymmetric geopotential height field, the mean asymmetric pressure gradient at the vortex center is defined as $\Delta\phi/D$, where $\Delta\phi$ and D are, respectively, the geopotential difference and the distance between the high and low asymmetric geopotential centers. The beta-drift speed C and the mean asymmetric pressure gradient $\Delta\phi/D$ for 14 cyclonic cases listed in Table 3a are well correlated with a linear correlation coefficient of 0.974 (Fig. 10a). The direction

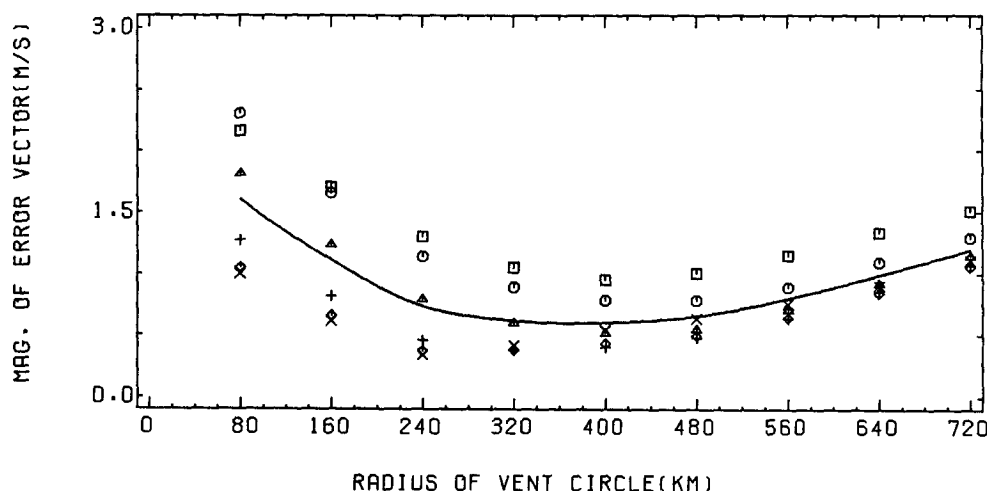


FIG. 6. The magnitude of error vector (MEV) at hour 24 as a function of radius of ventilation circle in the benchmark experiment. Symbols \square , \circ , \triangle , $+$, \times , and \diamond denote MEV at 175, 325, 475, 625, 775, and 925 mb, respectively. The solid line represents vertical mean MEV.

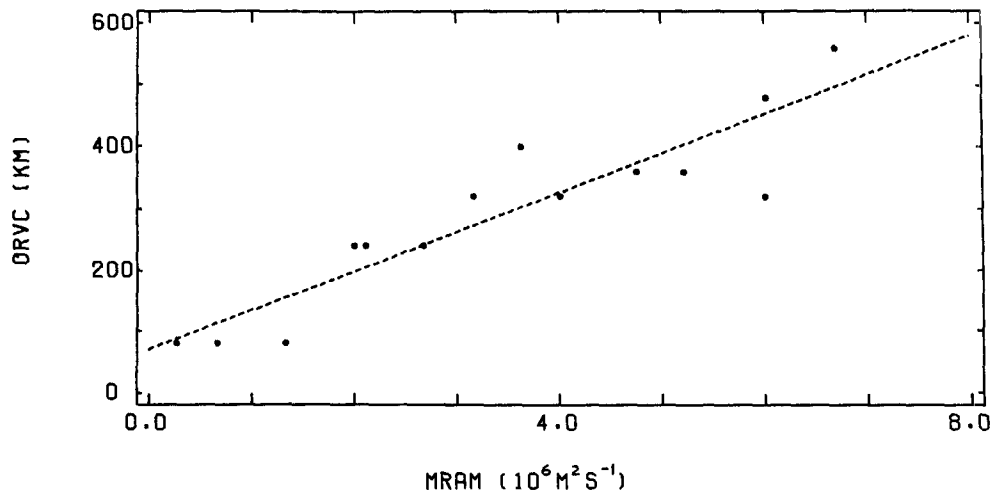


FIG. 7. Optimum radius of ventilation circle as a function of MRAM for 14 cyclonic cases (C1–C14 in Table 3a).

of the beta drift is also close to that of the corresponding geostrophic wind implied by the asymmetric pressure gradient force at the vortex center. The mean error for 14 cases is 9° with the mean geostrophic wind being to the right of the beta-drift velocity, and the standard deviation of the error is 9° .

For a vortex with height-dependent vertical structure, the relative angular momentum varies with height but the beta-drift velocity does not; rather it is determined by the vertical mean RAM. It is important to point out that the beta-induced asymmetric pressure gradient and the corresponding geostrophic wind at the vortex center also do not vary with height (Fig. 4b). This adds confidence to the correlation between asymmetric pressure field and vortex translation.

When horizontal structure of an initial vortex (thus, the mean relative angular momentum) changes, both the intensity of the asymmetric geopotential high and low and the distance between the high and low centers change accordingly. As a result, the beta-induced mean pressure gradient at the vortex center varies with the near-steady state or the initial MRAM. Figure 10b shows that the asymmetric pressure gradient $\Delta\phi/D$ is approximately proportional to the square root of the MRAM of the initial vortex. The dependence is essentially similar to that of beta drift speed on the MRAM (Fig. 3c). This suggests that the changes in MRAM due to changes in the vortex circulation structure may induce corresponding changes in the asymmetric pressure field. The latter influences the vortex translation.

c. Interpretation

To understand the relation between vortex translation and beta-induced asymmetric pressure field, consider the inviscid horizontal momentum equation

$$\frac{\partial \mathbf{V}}{\partial t} + \mathbf{V} \cdot \nabla \mathbf{V} + f \mathbf{k} \times \mathbf{V} = -\nabla \phi, \quad (8)$$

where \mathbf{V} is horizontal velocity and the vertical advection of momentum has been neglected.

The motion observed in a reference frame fixed to the earth may be expressed as

$$\mathbf{V} = \mathbf{C} + \mathbf{V}_s + \mathbf{V}_a, \quad (9)$$

where \mathbf{C} denotes the translation velocity of a cyclone, and \mathbf{V}_s and \mathbf{V}_a represent, respectively, the axially symmetric and asymmetric components of the cyclonic circulation observed in a system moving with the cyclone.

At the center of the cyclone, \mathbf{V}_s and the gradients of axisymmetric velocity and pressure all vanish. Thus, for steady translation substitution of (9) into (8) leads to

$$(\mathbf{C} + \mathbf{V}_a) \cdot \nabla \mathbf{V}_a + f \mathbf{k} \times (\mathbf{C} + \mathbf{V}_a) = -\nabla \phi_a, \quad (10)$$

where ϕ_a is the asymmetric geopotential field. Figure 8 indicates that in the vicinity of the cyclone center the magnitude of asymmetric rotational flow \mathbf{V}_a is only a small fraction of that of the beta-drift speed, hence $\mathbf{C} + \mathbf{V}_a$ can be approximated by \mathbf{C} . Furthermore, the characteristic scale of the asymmetric flow U is comparable to that of the beta-drift speed (Fig. 8). Assume R to be the characteristic length scale of the asymmetric flow, the ratio of the first term to the second term of (10) is U/fR (the Rossby number Ro). If typical values for $U = 2 \text{ m s}^{-1}$, $f = 0.4 \times 10^{-4} \text{ s}^{-1}$, and $R = 500 \text{ km}$, this ratio is 0.1. Thus, if $Ro \ll 1$, to the lowest order, (10) yields

$$\mathbf{C} = f^{-1} \mathbf{k} \times \nabla \phi_a, \quad (11)$$

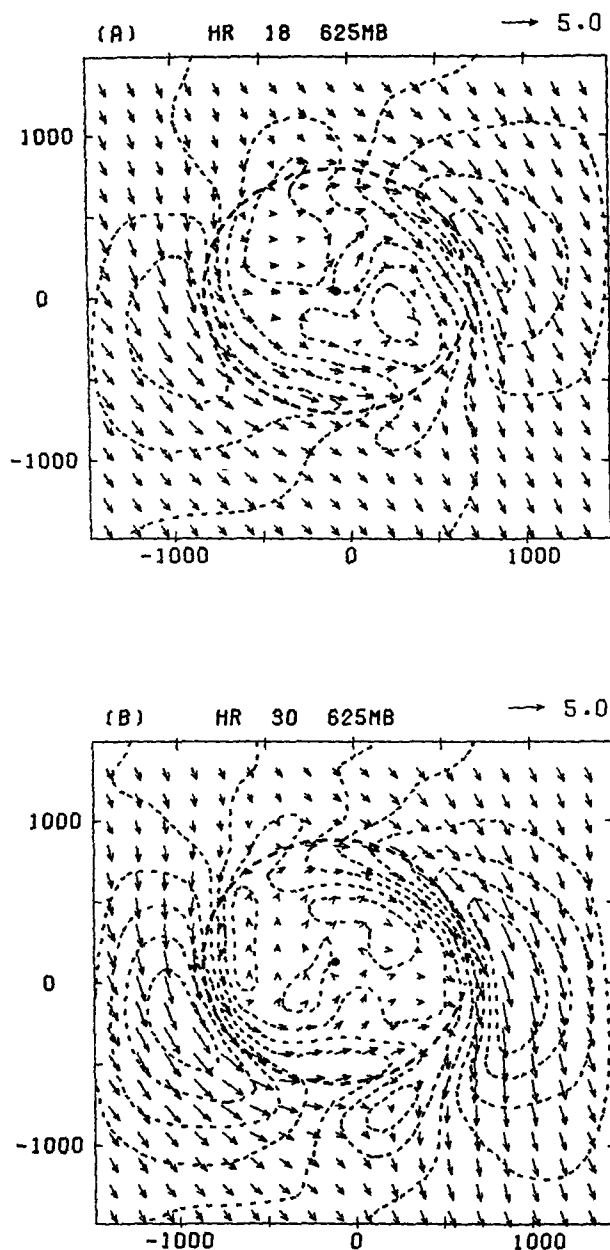


FIG. 8. The asymmetric flow field at 625 mb observed in a reference frame moving with the cyclone in the benchmark experiment at (a) hour 18 and (b) hour 30. The contours are isotachs whose interval is 0.5 m s^{-1} ; the closed dot denotes the vortex center and the thick dashed circle denotes the boundary of the cyclonic circulation of the vortex. Units of abscissa and ordinate are kilometers.

which states that the beta-drift velocity is approximately in geostrophic balance with the asymmetric geopotential field. This explains the relationship between the beta drift and the asymmetric pressure field obtained in our numerical experiments.

It has been demonstrated that the characteristics of the asymmetric pressure field are intimately associated with the mean relative angular momentum of the initial

vortex. It follows that the beta-drift speed should also correlate well with the MRAM of the initial vortex.

5. Conclusion and discussions

The movement of an initially isolated symmetric vortex embedded in a quiescent environment due to the interaction between the vortex circulation and the gradient of the earth's vorticity (the beta drift) was investigated via numerical experiments. The multilevel primitive equation model (a dry version of the FSU

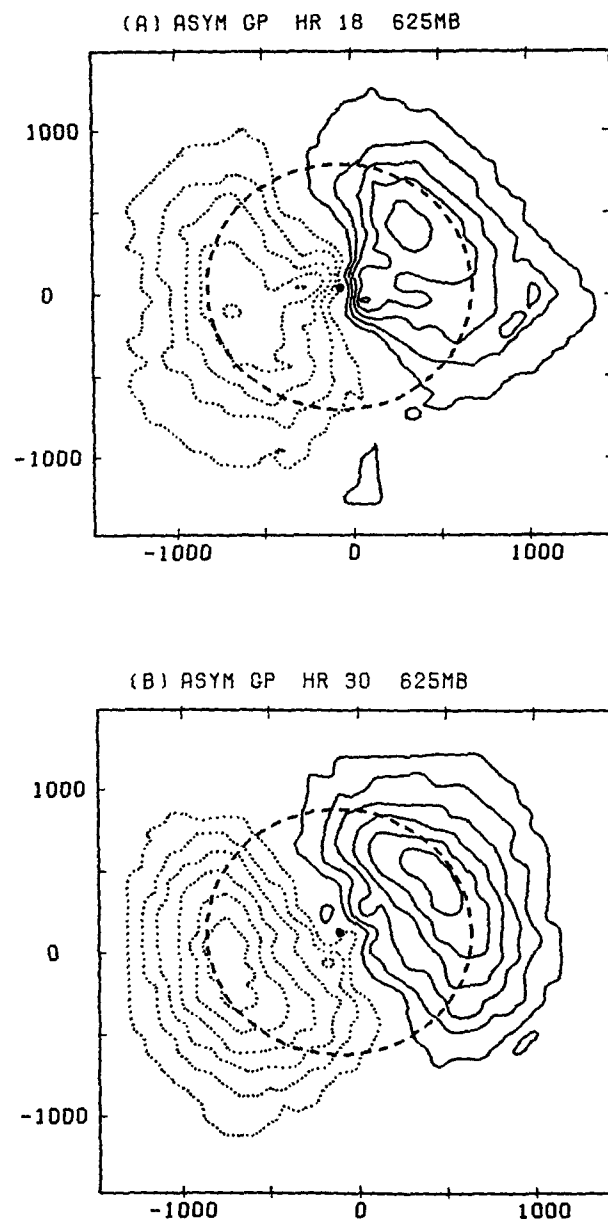


FIG. 9. As in Fig. 5, except for the asymmetric geopotential field. The contour interval is $10 \text{ m}^2 \text{ s}^{-2}$.

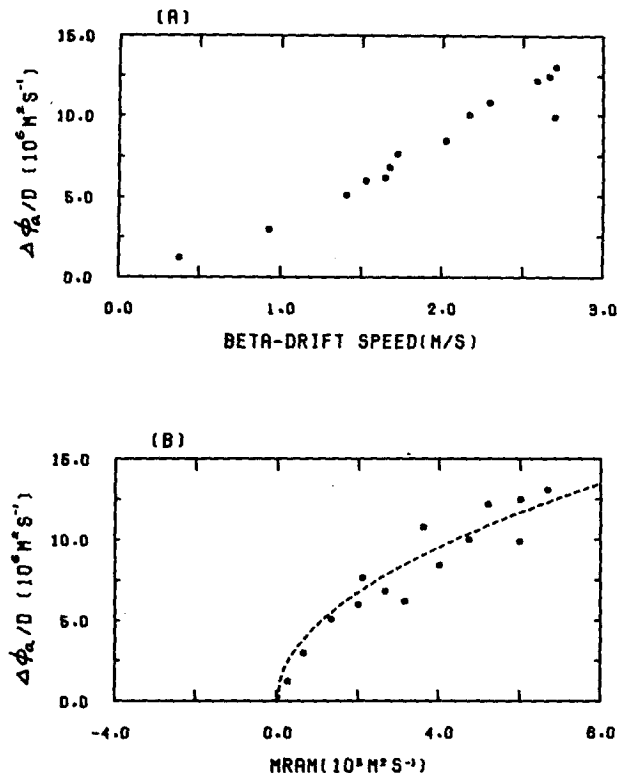


FIG. 10. Correlation diagrams between the beta-induced mean asymmetric geopotential gradient $\Delta\phi/D$ and (a) the beta-drift speed and (b) the MRAM of the initial vortex.

model) used in this study allows examination of the influences on vortex translation of both horizontal and vertical structures.

The cyclonic vortices initially (about 12 h) accelerate then translate quasi-steadily (Table 2a). Although the total relative angular momentum is not conserved due to Rossby wave dispersion, the mean relative angular momentum (MRAM) of the cyclonic circulation alone exhibits little change during the quasi-steady translation after an initial drop accompanying the acceleration (Table 2b). The ratio of MRAM at quasi-steady state to that of initial state is approximately a constant for different vortices used in our experiments. The weak anticyclonic circulation in the far-field outside the circle with a radius of $2R_0$ (R_0 being the initial vortex radius) has an insignificant effect on vortex translation in a 48-h integration. The existence of a quasi-steady phase of beta drift and the proportionality between initial and quasi-steady-state MRAM makes it meaningful to examine the relationship between the characteristics of the initial symmetric circulation and the quasi-steady vortex translation.

Differences in the meridional and zonal beta drift are noticeable. First of all, the sense of the meridional component of beta drift depends on the signs of both relative angular momentum and the Coriolis parameter

(the vertical component of the earth's vorticity): it is directed poleward for cyclones and equatorward for anticyclones. The zonal component of the beta drift, on the other hand, is always directed westward regardless of the signs of the relative angular momentum and the Coriolis parameter. Second, the poleward component of beta drift decreases significantly with increasing latitude, whereas the westward component does not have a simple relationship with the beta parameter or Coriolis parameter (Table 4). Lastly, the westward drift seems to be weakly linearly correlated with MRAM for selected samples (Fig. 3b), while the magnitude of the meridional drift speed is found to be roughly proportional to the square root of the MRAM of the initial vortex (Fig. 3a). These differences suggest that the meridional and zonal vortex translations are controlled by different physical processes. The westward drift, which is sensitive to vortex size and maximum winds within limited range, is related to beta-induced wave dispersion, which is directed westward. The meridional drift, which depends on the sense of the circulation and the Coriolis parameter, may be due to the Coriolis force and beta-induced pressure gradient force applied to the entire vortex. Both processes result from the meridional variation of planetary vorticity, an inherent property of the ambient medium. Since the poleward-drift speed is generally larger than the westward-drift speed for cyclonic vortices, the total beta-drift speed of a cyclone is also approximately proportional to the square root of the MRAM of the initial vortex [see (7)] and decreases with increasing latitude (Table 4).

The dependence of meridional beta drift on MRAM is clearly demonstrated for vortices whose tangential winds vary with height but do not reverse their sense. For these vortices, the area-averaged relative angular momentum at each level varies with height, but the beta-drift speed is nearly height independent (Fig. 4) and is determined by the vertical mean of the area-averaged RAM at each level; that is, the MRAM (Fig. 3a). This results from the vertical coupling of the vortex circulation by a secondary circulation developed in the deep cyclonic (or anticyclonic) vortex. It is also demonstrated that in the absence of the vertical coupling as in the case of a compound dry baroclinic vortex, the upper anticyclonic part translates southwestward, while the lower cyclonic part drifts northwestward for the Northern Hemisphere case.

The relationship between MRAM and the beta drift has practical implications. For vortices having similar strength measured by horizontal area-averaged RAM, the depth of the vortex is a crucial factor in considering its translation due to the beta effect: a deep vortex can be markedly faster than a shallow one. Further study of the beta drift in the presence of latent heat is necessary. In that case, the vertical coupling provided by latent heat-induced divergent circulation may effectively maintain the vortex as an integral system with

a coherent upper-level anticyclonic and lower-level cyclonic circulation. The opposite circulations aloft and below tend to have opposite meridional drifts that may compensate each other. The resultant beta drift is expected to be mainly westward or to substantially differ, in general, from that of a dry baroclinic vortex.

The beta effect interacting with an initial axisymmetric vortex circulation induces an axially asymmetric pressure field. There exists an intimate relationship between the asymmetric pressure field and beta drift. Our numerical experiments show that the asymmetric pressure field maintains a stationary pattern in azimuthal direction with a high pressure in the northeast and a low in the southwest quadrant (Fig. 9). Our experiments also reveal that for the vortices with height-dependent tangential wind (and angular momentum), the mean asymmetric pressure gradient at the vortex center does not vary with height, and the beta-drift speed is approximately proportional to the asymmetric pressure gradient at the vortex center.

Simple scale analysis shows that if the Rossby number associated with asymmetric motion is small, to the lowest order, the asymmetric pressure gradient force at the vortex center is balanced by the Coriolis force associated with the vortex translation. We speculate that if we approximate the vortex circulation as an idealized solid body, the asymmetric pressure field around the vortex would exert a resultant pressure gradient force to the vortex that is directed southwestward for a Northern Hemisphere cyclone. Rossby (1948) estimated the resultant environmental pressure gradient force on a solid-body-rotation vortex, which is directed westward and exactly balances the Coriolis force, so that the vortex moves northward. The translation of the cyclone is also subject to a Coriolis force. To the lowest order, the vortex translation will reach geostrophic balance as long as the Rossby number associated with asymmetric flow is small. In this sense, the beta drift may be viewed as a steady geostrophic motion implied by the beta-induced asymmetric pressure gradient force.

We have found that the asymmetric pressure gradient at the vortex center in the quasi-steady translation stage is roughly in proportion to the square root of the MRAM (Fig. 10b) and increases with the latitude where the vortex is located (Table 4). Further study is needed, however, to understand the nonlinear dependence of the beta-induced asymmetric pressure gradient at the vortex center upon the MRAM of the initial vortex and the Coriolis parameter. We intend to continue our study of these issues.

Acknowledgments. We wish to thank Prof. R. T. Williams for his insightful comments and suggestions that significantly improve the manuscript and Prof. T. N. Krishnamurti for providing us with FSU regional model that enables us to carry out this study. Thanks

are also extended to Prof. T. A. Schroeder for his comments, Dr. B. F. Abbey for providing the overall support of the Tropical Cyclone Motion Initiative, and Mr. M. Simpson for his technical assistance in optimization of the numerical codes. Computations were performed on the Alliant FX-8 at the School of Ocean and Earth Science and Technology (SOEST) computer Facilities and the CRAY X-MP48 at the San Diego Supercomputer Center. This research is supported by the Office of Naval Research under Grants N00014-88-K-0249 and N00014-90-J-1383.

REFERENCES

- Adem, J., 1956: A series solution for the barotropic vorticity equation and its application in the study of atmospheric vortices. *Tellus*, **8**, 364–372.
- Anthes, R. A., and J. E. Hoke, 1975: The effect of horizontal divergent and latitudinal variation of the Coriolis parameter on the drift of the model hurricane. *Mon. Wea. Rev.*, **103**, 757–763.
- Chan, J. C.-L., and R. T. Williams, 1987: Analytical and numerical studies of the beta-effect in tropical cyclone motion. Part I: Zero mean flow. *J. Atmos. Sci.*, **44**, 1257–1265.
- DeMaria, M., 1985: Tropical cyclone motion in a nondivergent barotropic model. *Mon. Wea. Rev.*, **113**, 1199–1209.
- Fiorino, M., and R. L. Elsberry, 1989a: Contributions to tropical cyclone motion by small, medium, and large scales in the initial vortex. *Mon. Wea. Rev.*, **117**, 721–727.
- , and —, 1989b: Some aspects of vortex structure related to tropical cyclone motion. *J. Atmos. Sci.*, **46**, 975–990.
- Frank, W. M., 1977: The structure and energetics of the tropical cyclone. I: Storm structure. *Mon. Wea. Rev.*, **105**, 1119–1135.
- Holland, G. J., 1983: Tropical cyclone motion: Environmental interaction plus a beta effect. *J. Atmos. Sci.*, **40**, 328–342.
- , 1984: Tropical cyclone motion: A comparison of theory and observation. *J. Atmos. Sci.*, **41**, 68–75.
- Jordan, C. L., 1958: Mean soundings for the West Indies area. *J. Meteor.*, **15**, 91–97.
- Kitade, T., 1981: Numerical experiments of tropical cyclones on a plane with variable Coriolis parameter. *J. Meteor. Soc. Japan*, **58**, 471–488.
- Krishnamurti, T. N., A. Kumar, K. S. Yap, A. P. Dartoor, N. Davison, and J. Sheng, 1990: Performance of high-resolution mesoscale tropical prediction model. *Adv. Geophysics*, **32**, 133–286.
- Madala, R. V., and S. A. Piacsek, 1975: Numerical simulation of asymmetric hurricane on a beta-plane with vertical shear. *Tellus*, **27**, 453–468.
- McCalpin, J. D., 1988: A quantitative analysis of the dissipation inherent in semi-Lagrangian advection. *Mon. Wea. Rev.*, **116**, 2330–2336.
- McWilliams, J. C., and G. R. Flierl, 1979: The evolution of isolated, nonlinear vortices. *J. Phys. Oceanogr.*, **9**, 1155–1182.
- Rossby, C. G., 1948: On displacement and intensity changes of atmospheric vortices. *J. Mar. Res.*, **7**, 175–196.
- Shapiro, L. J., and K. V. Ooyama, 1990: Barotropic vortex evolution on a beta plane. *J. Atmos. Sci.*, **47**, 170–187.
- Smith, R. K., W. Ulrich, and G. Dietachmayer, 1990: A numerical study of tropical cyclone motion using a barotropic model. I: The role of vortex asymmetries. *Quart. J. Roy. Meteor. Soc.*, **116**, 337–362.
- Wang, Y., and Y. Zhu, 1989: A numerical study on the Fujiwhara effect of two interacting cyclonic vortices. *J. Acad. Meteorol. Sci.*, **SMA**, **4**, 13–19. (in Chinese)
- Willoughby, H. E., 1988: Linear motion of a shallow-water, barotropic vortex. *J. Atmos. Sci.*, **45**, 1906–1928.